CHEMISTRY OF MATERIALS

Article

pubs.acs.org/cm

Ultramicroporous MOF with High Concentration of Vacant Cu^{II} Sites

Laura J. McCormick,[†] Samuel G. Duyker,[‡] Aaron W. Thornton,[§] Chris S. Hawes,[†] Matthew R. Hill,[§] Vanessa K. Peterson,[‡] Stuart R. Batten,[†,∥] and David. R. Turner*[,†]

[†]School of Chemistry, Monash University, Clayton, VIC 3800, Australia

[‡]Bragg Institute, Australian Nuclear Science and Technology Organisation, Locked Bag 2001, Kirrawee DC, NSW 2232, Australia

[§]CSIRO Materials Science and Engineering, Private Bag 33, Clayton South MDC, VIC 3169, Australia

[∥]Department of Chemistry, Faculty of Science, King Abdulaziz University, Jeddah, Saudi Arabia

Supporting Information

ABSTRACT: An ultramicroporous metal−organic framework (MOF) is reported that contains 0.35 nm nanotube-like channels with an unprecedented concentration of vacant Cu^{II} coordination sites. The nonintersecting, narrow channels in $[Cu_3(cdm)_4]$ (cdm = $C(CN)_2(CONH_2)^-$) align in two perpendicular directions, structurally resembling copper-doped carbon nanotubes with Cu^{II} embedded in the walls of the channels. The combination of ultramicroporosity with the exposed Cu^{II} coordination sites gives size-based selectivity of CO_2 over CH_4, based on pore-size distribution and modeling. Neutron powder diffraction and molecular dynamics simulations show the close packing of single rows of guests within the tubular nanostructure and interaction of CO_2 with the exposed metal sites.

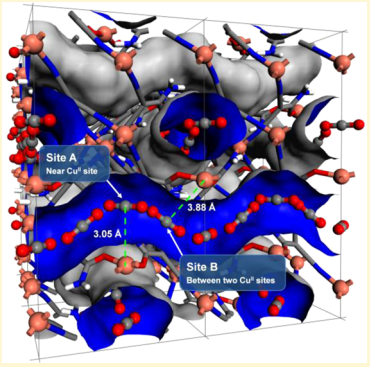

INTRODUCTION

Two of the most studied materials for storage and sensing of small molecules in current research are metal−organic frameworks (MOFs) and carbon nanotubes (CNTs).[1−3] These materials have found particular use in selective adsorption and detection of gaseous analytes, with attention on H_2 or CO_2 storage.[4,5] Nanotubes in particular have been used for sensing based on changes in resistivity.[6] Despite some similarities between MOFs and CNTs, i.e., large internal surface areas and guest-accessible channels, they display markedly different gas uptake behavior. MOFs tend to possess complex pore topologies, typically 3D in nature, allowing exchange of adsorbed species and pathways through the material.[7] These pores are typically in the 1−2 nm size range and are tailorable through judicious selection of components used.[8] Conversely, CNTs contain only a 1D channel and have relatively poor adsorption behavior due to their weak interactions with gases.[9] The uptake properties can be enhanced by incorporation of sites with stronger affinities for gaseous guests, such as by doping metal ions into the nanotubes.[10] Nanotubes also have a lack of size control below ca. 1 nm, thereby giving poor size-based selectivity, and there is difficulty in aligning the tubes in bulk samples in order to take advantage of any potential separation applications.

Coordination polymers, of which MOFs represent a significant subset,[11] can be rationally designed as proposed by Robson.[12] Some significant advantages of MOFs with regards to providing strong host−guest interactions are their ability to be synthetically modified to expose bare metal sites,[13] chemical reduction of the framework by metalation, cation exchange,[14] or the addition of internal pendant groups.[15−17] MOFs are also able to display pore-size control that cannot be reliably achieved with CNTs and that has been shown to be very beneficial for CO_2 capture if pore size is complementary to the kinetic diameter of CO_2.[18−21] It has been postulated recently that it should be possible to reliably access metal−organic materials (MOMs) that display nanotube-like structure and behavior, which have been termed SWMONTs (single-walled metal organic nanotubes).[22] While reports of tubular metal−organic materials are relatively rare, an alternative strategy of great promise is the synthesis of more traditional MOFs with arrays of nonintersecting 1D channels. Size control is again important, and there is currently considerable interest in ultramicroporous MOMs, which possess channels with internal diameters <0.7 nm (i.e., smaller than an N_2 bilayer).[23] Such small pores can lead to highly selective sorption by size discrimination and display unique sorption properties, including significant pore-blocking at low temperatures and quantum effects on guest sorption.[3,24−29]

We report here a unique mixed-valent copper framework containing ultramicroporous, nonintersecting 1D channels in two directions with an unprecedented density of vacant Cu^{II} sites embedded within the walls. The material has been shown by neutron powder diffraction and molecular dynamics (MD) simulations to host CO_2 in tight confines close to these metal

Received: June 17, 2014
Published: July 15, 2014

   dx.doi.org/10.1021/cm502189c | Chem. Mater. 2014, 26, 4640−4646

sites, with guest orientation largely dictated by the size of the channels, and to display size-dependent adsorption of CO_2 over CH_4.

EXPERIMENTAL SECTION

Synthesis. K(cdm) was prepared according to a literature procedure.[30] K(cdm) (240 mg, 1.63 mmol) was almost completely dissolved in methanol (30 mL) with the aid of sonication. To this was added a methanolic solution (3 mL) of anhydrous $CuCl_2$ (216 mg, 1.61 mmol). Upon the addition of the green $CuCl_2$ solution, the remaining suspended K(cdm) was dissolved to give a deep orange solution. Dark orange crystals of solvated $[Cu_3(cdm)_4]$ (173 mg, 0.252 mmol, 62% yield) formed on the walls of the reaction vessel over a period of 2 days. Elemental analysis calcd. for $Cu_3(C_4H_2N_3O)_4 \cdot 2MeOH \cdot 1.5H_2O$ ($C_{18}H_{19}N_{12}Cu_3O_{7.5}$): C, 30.28; H, 2.68; N, 23.54. Found: C, 29.99; H, 2.30; N, 23.59%. Powder diffraction confirms a phase-pure product. Thermogravimetric analysis (Figure S1, Supporting Information) shows 12.5% weight loss before decomposition at ca. 230 °C, calculated 12.8% for loss of all solvent from $Cu_3(C_4H_2N_3O)_4 \cdot 2MeOH \cdot 1.5H_2O$.

X-ray Crystallography. A suitable single crystal was mounted on a fine glass fiber using viscous hydrocarbon oil. Data were collected using a Bruker X8 Apex2 diffractometer equipped with graphite monochromated Mo−Kα radiation (λ = 0.71073 Å). The data collection temperature was maintained at 123 K using an open-flow N_2 cryostream. Data reduction was carried out using the Bruker Apex2 software suite.[31] The structure was solved by direct methods using SHELXS-2013.[32] Refinement was carried out against F^2 using SHELXL-2013.[33] All non-hydrogen atoms were refined using an anisotropic model. Hydrogen atoms belonging to the amide group were placed in idealized X-ray positions and refined using a riding model. Solvent coordinated to the Cu(II) was modeled as 50:50 H_2O/MeOH. Additional refinement details are supplied in the Supporting Information.

Crystal data for $[Cu_3(cdm)_4(H_2O)(MeOH)]$: $C_{17}H_{13}Cu_3N_{12}O_6$, M = 672.01, orange block, 0.140 × 0.120 × 0.120 mm^3, $I\bar{4}2d$ space group (No. 122), V = 2737.7(3) Å^3, Z = 4, D_c = 1.630 g/cm^3, F_{000} = 1336, $2\theta_{max}$ = 55.0°, 5238 reflections collected, 1561 unique (R_{int} = 0.0313). Final *GooF* = 1.119, R_1 = 0.0472, wR_2 = 0.1336, R indices based on 1431 reflections with $I > 2\sigma(I)$ (refinement on F^2), 90 parameters, 1 restraint, μ = 2.363 mm^{-1}. CCDC 1000273.

Neutron Powder Diffraction. Neutron powder diffraction data were collected on the high-intensity neutron diffractometer, Wombat (OPAL, ANSTO, Australia).[34] Prior to neutron powder diffraction measurement and gas dosing, 1.119 g of desolvated $[Cu_3(cdm)_4]$ was transferred to a cylindrical vanadium can (internal diameter of ca. 6 mm) inside a helium-filled glovebox equipped with water and oxygen monitors. The sample cell was connected to a custom-designed gas-delivery center-stick and inserted into a top-loading cryofurnace. Temperature control at the sample was achieved using cartridge heaters and silicon-diode temperature sensors at the top and bottom of the cell. The gas-delivery line was also temperature-controlled in order to avoid freezing CO_2 inside the tube, so that the sample could be left in place throughout the experiment without the requirement of warming the entire cryofurnace between gas doses. An initial diffraction pattern was collected on the evacuated sample at 15 K to be used as a structural reference point from which subsequent data for the CO_2-dosed sample could be analyzed. The sample was then warmed to 300 K prior to dosing with a known amount of CO_2, before being slowly cooled to the measurement temperature of 15 K, all the while ensuring that the temperature was kept above the boiling/sublimation point of CO_2 at the current pressure. By 150 K the pressure reading was zero, indicating that all CO_2 had been absorbed by the sample. No evidence of frozen CO_2 was observed in the diffraction patterns. The total cooling time was approximately 1 h, with the intention of ensuring diffusion of the CO_2 molecules to their thermodynamic equilibrium positions and minimizing random disorder of guest molecules prior to the diffraction measurement. Thirty minutes of diffraction data were acquired for each dose using an area detector in the angular range 17° < 2θ < 137° with an incident neutron wavelength of 2.4145(3) Å, determined using an Al_2O_3 standard reference material (NIST SRM 676). A correction was applied to the Debye−Scherrer ring curvature before data reduction.

Rietveld analysis and difference Fourier analysis of the diffraction data was carried out using GSAS and EXPGUI,[35,36] with a pseudo-Voigt peak shape and 16-term shifted Chebyshev background function. VESTA was used for visualization of the crystal structure and nuclear density isosurfaces.[37] Following refinement of the guest-free structure, this was used together with the data from the CO_2-loaded sample to generate Fourier difference maps of residual nuclear density. Further details are provided in the Supporting Information.

Calculations. The static cavity size distribution was calculated using the geometric sizing algorithm using atomic coordinates from the single crystal data.[38] There is a dominant cavity size of around 3.9 Å that represents the main channels. Using molecular dynamics (MD) with generic UFF, the flexibility of the channel size was investigated over one nanosecond at 123 K with fixed cell volume. The window size was defined as the maximum size of a spherical probe allowed to pass through the structure.[39] All DFT calculations were performed using VASP 5.2 with the Perdew−Burke−Ernzerhof (PBE) generalized gradient approximation (GGA) functional and Gaussian smearing of partial occupancies (see Supporting Information for full experimental details).

RESULTS AND DISCUSSION

Synthesis and Structure. The mixed-valent Cu^I/Cu^{II} coordination polymer $[Cu_3(cdm)_4(MeOH)(H_2O)]$ was synthesized by reaction of K(cdm), where cdm is the dinitrile anion $C(CN)_2(CONH_2)^-$, with $CuCl_2$ in aerobic conditions following from our extensive work on discrete coordination complexes using this ligand[40] (full synthetic details in Supporting Information). Mixed-valent coordination polymers of copper are not unknown, with precedents typically being materials containing cyanide, halide, azide, or thiocyanate bridging ligands. Powder diffraction confirms that the synthesis gives a phase-pure product (see Supporting Information). Elemental analysis and thermogravimetric analysis (TGA) indicate that both water and methanol are present within the as-synthesized material. In part these solvents are coordinated, although the proportion of coordinated MeOH/H_2O is difficult to determine crystallographically as the solvent lies on a crystallographic 4-fold axis.

The material crystallizes in the tetragonal space group $I\bar{4}2d$ with a single cdm ligand in the asymmetric unit, the Cu^{II} atoms residing on a rotoinversion site and the Cu^I atoms lying on rotation axes. The Cu^I atoms are tetrahedral and are exclusively coordinated by nitrile groups. The Cu^{II} atoms are octahedral with four κO-cdm ligands in the equatorial positions and coordinated solvent, a mixture of MeOH and H_2O, in the axial positions. Both metals therefore act as four-connecting nodes. The cdm ligand is a three-connecting node giving the structure an overall self-penetrating $(8^2.10)_4(8^3.10^3)_2(8^5.10)$ topology (Supporting Information, Figure S2). The closely related anions dicyanamide (dca) and tricyanomethanide (tcm) are both known to form 3D structures in binary complexes, although in these instances the metal coordination spheres are filled completely by the ligands and typically give close-packed structures.[40] The mixed nitrogen/oxygen donor groups in cdm, alongside the mixed Cu^I/Cu^{II} present in the structure, mean that the metal/donor preferences are ideal for easily removed solvent to be present in the axial Cu^{II} sites, thereby allowing guest-accessible pores. The short distance between the donor atoms is ideal for forming ultramicroporous channels.

dx.doi.org/10.1021/cm502189c | Chem. Mater. 2014, 26, 4640−4646

Nonintersecting, nanotube-like channels run through the structure parallel to the crystallographic *a* and *b* axes (Figure 1).

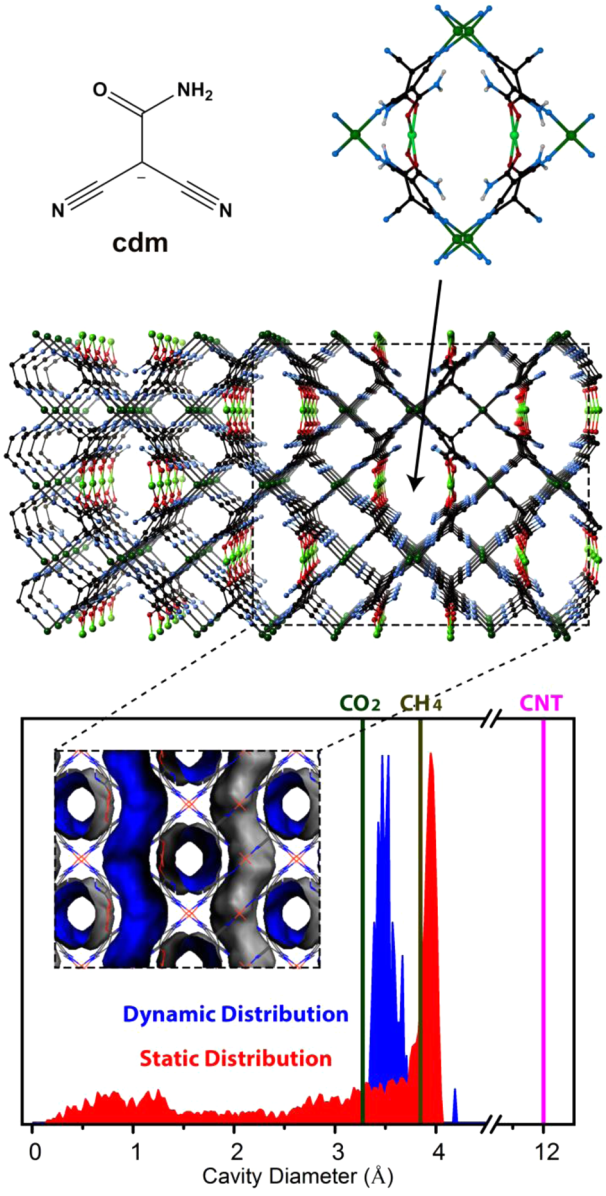

Figure 1. Ultramicroporous structure of $[Cu_3(cdm)_4]$ contains nonintersecting channels with a dynamic diameter fluctuating around 3.5 Å, intermediate between the kinetic diameters of CH_4 and CO_2, and significantly smaller than the smallest reported CNT.

In the as-synthesized material, axially coordinated solvent on the Cu^{II} atoms protrudes into these narrow channels, effectively blocking them for any application. The most striking feature of these 1D channels is the high density of vacant Cu^{II} coordination sites that is present once the solvent has been removed, with open-metal sites known to enhance interactions with gases.[41] These metal sites occupy opposing walls of the channels and are spaced apart by ca. 11.2 Å along one wall. Taking into account the two Cu^{II}-lined walls this gives a vacant metal site every 5.6 Å along the channels, with the closest Cu···Cu distance being 7.8 Å (cf. 8.0 Å in the narrow "windows" in the structure of HKUST-1).[42] Further potential points of interaction for guest molecules are provided by the NH_2 group of the ligands, which protrudes very slightly into the channels at a similar spacing. The extremely small size of the channels is obtained by the use of the cdm ligand, which is itself small and sterically undemanding, with only single atoms as points of coordination to the metals. Thus, this ligand has advantages over larger, more complicated ligands that rely on bulkier coordinating groups, such as pyridine, which crowd the immediate metal coordination sphere. The small bridging distance between the coordinating groups of the cdm ligand, with the three Cu···Cu distances around one ligand in the range 6.36−8.26 Å, is ideal for forming an ultramicroporous material.

The static cavity size distribution for these channels was calculated using a geometric sizing algorithm, showing a dominant cavity size of ca. 3.9 Å that represents the main channels in the structure (Figure 1).[43] The flexibility of these channels was investigated using molecular dynamics simulations over 1 ns with the generic universal force field (UFF, Figure 1).[44] The window size in the MD simulations was defined by the maximum size of a spherical probe that is allowed to pass through the channel. Over the course of this simulation the window size fluctuated around 3.5 Å, suggesting that the material may have a potential sieving mechanism as the channel size lies intermediate between that of CO_2 (kinetic diameter = 3.3 Å) and CH_4 (kinetic diameter = 3.87 Å). The remarkably small internal size of these channels is significantly smaller than those in the ultramicroporous salen-derived MOF of Chen et al. (5.6 × 12.0 Å), which also contains vacant Cu^{II} coordination sites,[24] and marginally smaller than those in the SIFSIX-3 MOM (ca. 3.8 Å at low temperatures).[19,25,45]

Gas Sorption Experiments. The coordinated solvent molecules, and uncoordinated solvent within the channels, can be removed by treatment of the material with supercritical CO_2 ($scCO_2$), well-known as an effective method of MOF activation,[46] to give the desolvated framework $[Cu_3(cdm)_4]$. Retention of crystallinity upon desolvation was demonstrated by neutron powder diffraction (NPD, Figure 2).

Studies of the gas sorption properties of the material were conducted for CO_2, CH_4, H_2, and Ar (Figure 3; full details in Supporting Information). At 273 K almost twice as much CO_2 is taken up as CH_4 (46 $cm^3\ g^{-1}$ vs 25 $cm^3\ g^{-1}$ at 1000 mbar) bearing out the prediction from the MD simulations that the size of the pore may lead to sieving or selective adsorption between these two gases. While increased uptake of CO_2 is not unexpected for most MOFs,[1,3] it is uncommon for the cavity diameter to be intermediate between that of the two gases. Uptake of hydrogen and argon are negligible at 77 and 87 K, respectively, with nitrogen also not adsorbed at similar temperatures. Such sorption behavior is known for ultramicroporous MOFs/MOMs.[3,32] The adsorption kinetics are also remarkably slow, with CO_2 sorption at 273 K requiring 68 h to reach saturation (Supporting Information, Figure S12) giving further evidence of sieving kinetics even at relatively high temperatures.

Predictions of the adsorption behavior were conducted using grand canonical Monte Carlo (GCMC) simulations (Figure 3). These simulations overestimate the experimental isotherms although the general trends that are observed are captured. It appears that the size, shape, and charge composition of CO_2 is much more favorable for adsorption within the channels than CH_4, with twice as many molecules of CO_2 being taken in. Calculations of experimental enthalpies are unreliable due to step-like behavior at low pressures, indicative of the tube-like adsorption (see Supporting Information, Figure S11). The predicted and experimentally determined uptake of H_2 is less

dx.doi.org/10.1021/cm502189c | *Chem. Mater.* 2014, 26, 4640−4646

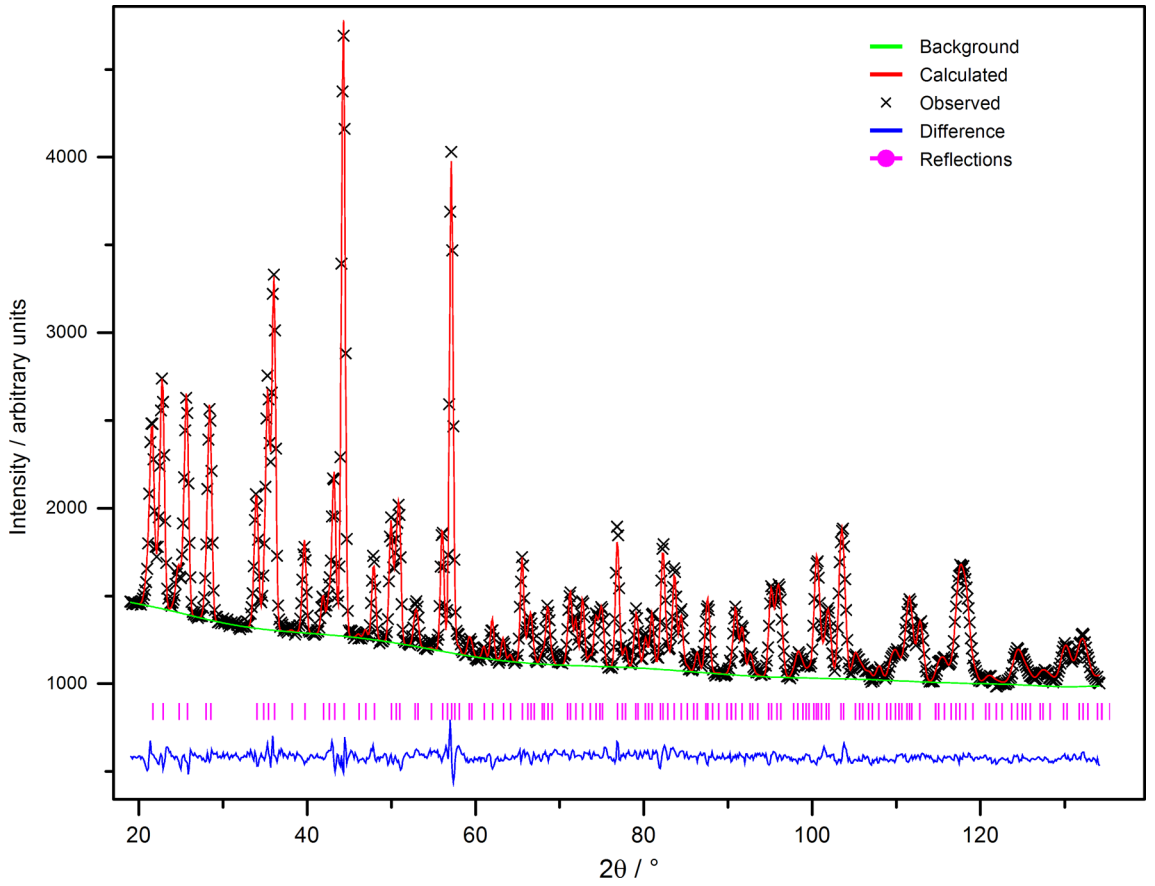

Figure 2. Rietveld refinement (red) against NPD data (black) for guest-free $[Cu_3(cdm)_4]$ at 15 K after activation by supercritical CO_2.

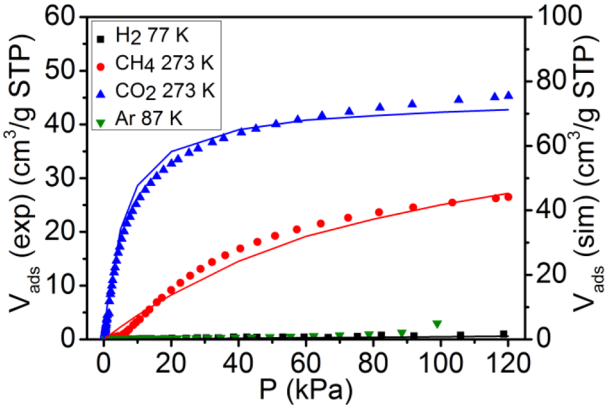

Figure 3. Experimental (icons) and simulated (solid lines) sorption traces highlighting the difference in behavior between CO_2 and CH_4 and negligible uptake of Ar and H_2.

than 1 $cm^3\ g^{-1}$. The postulated reason for this low uptake is a quantum effect that occurs due to nanoscale confinement of light gases. The enormous reduction in predicted H_2 uptake is accounted for by incorporating the quantum Feynman–Hibbs potential into calculations (see Supporting Information, Figure S13).[47,48] Similar behavior is observed for other ultra-microporous materials, including the recent NOTT-300 material, which has somewhat larger (ca. 6.5 × 6.5 Å) pores.[49] The difference in adsorption between CH_4 and CO_2 in $[Cu_3(cdm)_4]$ was further investigated by fitting the experimental isotherms with the dual Langmuir expression and utilizing the ideal adsorbed solution (IAST) model to predict mixed-gas isotherms of various industrially relevant compositions (see Supporting Information).[50,51] These results suggest that there is good selectivity for CO_2 over CH_4 under the conditions that were modeled, although higher selectivities are known.[52]

Neutron Powder Diffraction. To explore the host–guest interactions within the material, neutron powder diffraction (NPD) experiments with in situ gas loading were performed using the Wombat diffractometer at ANSTO.[34] An initial diffraction pattern from $scCO_2$-activated and evacuated $[Cu_3(cdm)_4]$ at 15 K was used as a structural reference point for analysis of the CO_2-loaded structures with Rietveld refinement giving a low R value with no evidence of residual solvent (Figure 2). The sample was treated with two successive doses of CO_2 with loadings of 1.00 and 2.00 CO_2/$[Cu_3(cdm)_4]$. Slow uptake during the final part of the second gas dose indicated that the sample was reaching its maximum CO_2 capacity. The final quantity of adsorbed CO_2 was equivalent to 73 $cm^3\ g^{-1}$ at STP, which, due to the lower temperature involved, is considerably greater than the uptake measured at 1 bar and 273 K. No new reflections were observed in the CO_2-loaded diffraction patterns, indicating that the original symmetry is preserved.

Fourier-difference analysis of the NPD data revealed two CO_2 sites within the channels (Figure 4). Site A, which at the 1 CO_2/$[Cu_3(cdm)_4]$ loading level contains the most nuclear density, is close to the open Cu^{II} site with the residual density suggestive of CO_2 lying side-on to the metal. CO_2 typically binds in an end-on fashion,[53−55] but in the present case this arrangement would align poorly with the geometry of the

dx.doi.org/10.1021/cm502189c | Chem. Mater. 2014, 26, 4640−4646

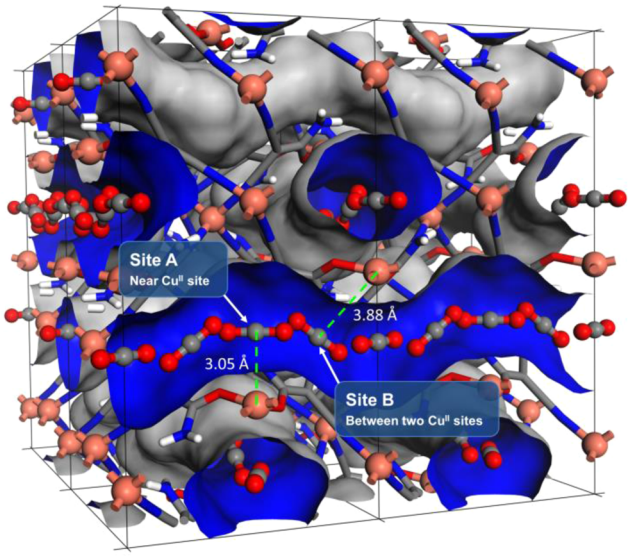

Figure 4. Two distinct adsorption sites in CO_2-loaded $[Cu_3(cdm)_4]$, as determined by the combination of NPD and DFT calculations. The labeled distances are from the Rietveld refinement for $[Cu_3(cdm)_4]\cdot 1CO_2$. Because of the short distance between the two sites, both cannot be simultaneously filled as shown.

channel, whereas the side-on orientation enables increased interaction with the pore walls. Site B is located in the narrower part of the channel, midway between two diagonally opposite open Cu^{II} sites. The constricted pore environment does not appear to allow the geometric arrangement necessary for a strong interaction between CO_2 molecules and the NH_2 groups, and no significant residual nuclear density was found in their vicinity.

The somewhat diffuse nuclear density at these sites indicates some positional disorder of the CO_2 molecules, despite confinement by the small channels. A single partially occupied CO_2 molecule in the side-on arrangement was satisfactorily modeled at site A, with refined occupancies of 0.35 and 0.40 for the C and O atoms, respectively. A single 0.15 occupancy C atom was modeled at the center of the residual density at site B, but as a consequence of the disorder, the corresponding oxygen atoms of the CO_2 are not readily located. The relative ease of locating this C atom implies that the orientation of the CO_2, rather than its center of mass, is disordered. The combined C occupancies at the two sites are in good agreement with the dosed amount for both loading levels (Table 1). The occupancy of site A increases only slightly at higher loading, indicating that it is nearly saturated by the first dose, while the site B occupancy increases significantly. The overall result is roughly half-filling of each site at the higher CO_2 loading.

Table 1. Refined Occupancies and Distances from the Nearest Cu^{II} Site for the Two Unique CO_2 Adsorption Sites in $[Cu_3(cdm)_4]$ (1)

	CO_2 occupancy			Cu···C (Å)	
CO_2:1 dosed	site A[a]	site B[b]	CO_2:1 found	site A	site B
0	0	0	0		
1.00	0.37(6)	0.147(29)	1.04(13)	3.0465(5)	3.8788(4)
2.00	0.43(8)	0.55(6)	1.97(20)	3.0926(6)	3.8923(4)

[a]Based on C and O occupancies. [b]Based on C occupancy.

DFT-based MD simulations at 100 K were performed to validate the NPD experimental results and determine the orientation of the CO_2 molecules. The time-averaged site A position in the MD simulation is in good agreement with the NPD data with CO_2 side-on to the metal. The simulation shows CO_2 molecules moving back and forth between sites A and B and provides strong evidence that the preferred orientation of the CO_2 molecule at both sites is along the direction of the channel. The motion is rapid even at 100 K, with each CO_2 molecule switching sites an average of three times during the 25 ps simulation, indicating a small energy difference between the two sites. When occupying site B, the CO_2 molecules are located with their C atoms midway between the two Cu sites, in good agreement with the C position refined from the NPD data.

DFT structure relaxation at 0 K was performed in order to clarify the most energetically favorable arrangement for CO_2 molecules at each site. The optimized arrangement for CO_2 in site A is in good agreement with the side-on orientation observed in the Rietveld refined NPD structure. The calculated Cu···C distance of 3.76 Å is longer than that observed experimentally, likely a result of the fact that DFT does not account for van der Waals interactions.

The distance of 7.78 Å between open Cu^{II} sites on either side of site B is comparable to the 7.15 Å distance between open metal sites in the $Co_3[Fe(CN)_6]_2$ Prussian blue analogue (PBA) in which a bridging CO_2 binding mode was recently established.[56] $[Cu_3(cdm)_4]$ provides a second example of a CO_2 molecule interacting with two bare metal sites, although due to the highly constricted pore environment, the CO_2 is unable to adopt a similar binding mode to that in the PBA. All DFT energy minimizations in which a CO_2 molecule was initially placed in site B and end-on to the two Cu^{II} sites quickly resulted in the molecule returning to an orientation parallel to the channel, indicating that such an end-on bridging mode carries a large energy penalty due to the narrowness of the channels. The channel-aligned arrangement yields a longer M–CO_2 distance than in the PBA (M···C = 3.89 Å) but enables greater interaction with the channel walls.

The simultaneous occupation by CO_2 of both an A-site and the adjacent B-site is not energetically favorable due to the short guest–guest distances that this would entail (O···O ≈ 1.0 Å), thereby limiting the CO_2 capacity of the framework with each site only ca. 50% occupied at the maximum achieved loading of 2.0 $CO_2/[Cu_3(cdm)_4]$. The small energy difference (calculated to be 2 kJ mol^{-1}) between the two sites means that they both compete relatively equally to bind CO_2. Additionally, once 50% occupancy is reached at site A, there is on average one CO_2 molecule interacting with each Cu^{II} ion, which is likely to alter the energetics of this site and reduce the likelihood of another molecule interacting with the opposite axial site of the same Cu^{II} ion. Site B could then become the more favorable site and subsequently fill until the aforementioned steric limit of 2.0 $CO_2/[Cu_3(cdm)_4]$ is reached. This filling regime is supported by the changes in the adsorption site occupation from NPD experiments.

CONCLUSIONS

The ultramicroporous structure of $[Cu_3(cdm)_4]$, which contains 0.35 nm nonintersecting channels combined with close vacant Cu^{II} sites lining the internal walls, has been shown to display selective gas uptake of CO_2. The internal pore size is ideal for improved sorption of CO_2 over CH_4 with a dynamic

dx.doi.org/10.1021/cm502189c | Chem. Mater. 2014, 26, 4640–4646

diameter intermediate between the kinetic radii of the two gases, although the tight confines of the 1D channel results in slow kinetics. Gas sorption experiments, supported by GCMC simulations, show that the uptake of CO_2 is almost twice that of CH_4 up to a pressure of 1000 mbar. There is negligible uptake of H_2 arising from a quantum effect. Neutron powder diffraction and DFT/MD calculations show the interaction of CO_2 at two positions close to the open metal sites, aligned with the direction of the narrow channels. The system demonstrates the influence of free metal sites for CO_2 binding, and calculations suggest a significant role of the channel size in separations.

■ ASSOCIATED CONTENT

Ⓢ Supporting Information

Expanded experimental section and data (X-ray, NPD, gas sorption, DFT, and modeling). This material is available free of charge via the Internet at http://pubs.acs.org.

■ AUTHOR INFORMATION

Corresponding Author

*(D.R.T.) E-mail: david.turner@monash.edu.

Author Contributions

The manuscript was written through contributions of all authors.

Notes

The authors declare no competing financial interest.

■ ACKNOWLEDGMENTS

The authors acknowledge the Science and Industry Endowment Fund (SIEF) and the Australian Institute of Nuclear Science and Engineering for funding. D.R.T. and M.R.H. acknowledge the Australian Research Council for Future Fellowships. Part of this work was conducted at the Bragg Institute under proposal PP2548.

■ REFERENCES

(1) Bae, Y. S.; Snurr, R. Q. *Angew. Chem., Int. Ed.* **2011**, *50*, 11586.
(2) Chen, B.; Xiang, S.; Qian, G. *Acc. Chem. Res.* **2010**, *43*, 1115.
(3) D'Alessandro, D. M.; Smit, B.; Long, J. R. *Angew. Chem., Int. Ed.* **2010**, *49*, 6058.
(4) Yaghi, O. M.; Li, G. M.; Li, H. L. *Nature* **1995**, *378*, 703.
(5) Sumida, K.; Rogow, D. L.; Mason, J. A.; McDonald, T. M.; Bloch, E. D.; Herm, Z. R.; Bae, T.-H.; Long, J. R. *Chem. Rev.* **2012**, *112*, 724.
(6) Kong, J.; Franklin, N. R.; Zhou, C. W.; Chapline, M. G.; Peng, S.; Cho, K. J.; Dai, H. J. *Science* **2000**, *287*, 622.
(7) Batten, S. R.; Neville, S. M.; Turner, D. R. *Coordination Polymers: Design, Analysis and Application*; The Royal Society of Chemistry: Cambridge, U.K., 2009.
(8) Zhao, D.; Timmons, D. J.; Yuan, D. Q.; Zhou, H. C. *Acc. Chem. Res.* **2011**, *44*, 123.
(9) Zhao, J. J.; Buldum, A.; Han, J.; Lu, J. P. *Nanotechnology* **2002**, *13*, 195.
(10) Ang, L. M.; Hor, T. S. A.; Xu, G. Q.; Tung, C. H.; Zhao, S. P.; Wang, J. L. S. *Carbon* **2000**, *38*, 363.
(11) Batten, S. R.; Champness, N. R.; Chen, X. M.; Garcia-Martinez, J.; Kitagawa, S.; Ohrstrom, L.; O'Keeffe, M.; Suh, M. P.; Reedijk, J. *Pure Appl. Chem.* **2013**, *85*, 1715.
(12) Robson, R. *Dalton Trans.* **2008**, 5113.
(13) Mallick, A.; Saha, S.; Pachfule, P.; Roy, S.; Banerjee, R. *J. Mater. Chem.* **2010**, *20*, 9073.
(14) An, J.; Rosi, N. L. *J. Am. Chem. Soc.* **2010**, *132*, 5578.
(15) Bae, Y. S.; Farha, O. K.; Hupp, J. T.; Snurr, R. Q. *J. Mater. Chem.* **2009**, *19*, 2131.
(16) Arstad, B.; Fjellvåg, H.; Kongshaug, K. O.; Swang, O.; Blom, R. *Adsorption* **2008**, *14*, 755.
(17) Si, X. L.; Jiao, C. L.; Li, F.; Zhang, J.; Wang, S.; Liu, S.; Li, Z. B.; Sun, L. X.; Xu, F.; Gabelica, Z.; Schick, C. *Energy Environ. Sci.* **2011**, *4*, 4522.
(18) Li, J.-R.; Yu, J.; Lu, W.; Sun, L.-B.; Sculley, J.; Balbuena, P. B.; Zhou, H.-C. *Nat. Commun.* **2013**, *4*, 1538.
(19) Nugent, P.; Belmabkhout, Y.; Burd, S. D.; Cairns, A. J.; Luebke, R.; Forrest, K.; Pham, T.; Ma, S.; Space, B.; Wojtas, L.; Eddaoudi, M.; Zaworotko, M. J. *Nature* **2013**, *495*, 80.
(20) Wriedt, M.; Sculley, J. P.; Yakovenko, A. A.; Ma, Y.; Halder, G. J.; Balbuena, P. B.; Zhou, H.-C. *Angew. Chem., Int. Ed.* **2012**, *51*, 9804.
(21) Xiang, S.; He, Y.; Zhang, Z.; Wu, H.; Zhou, W.; Krishna, R.; Chen, B. *Nat. Commun.* **2012**, *3*, 954.
(22) Thanasekaran, P.; Luo, T.-T.; Lee, C.-H.; Lu, K.-L. *J. Mater. Chem.* **2011**, *21*, 13140.
(23) Lowell, S.; Shields, J. E.; Thomas, M. A.; Thommes, M. *Characterization of Porous Solids and Powders: Surface Area, Pore Size and Density*; Kluwer Academic Publishers: Dordrecht, The Netherlands, 2004.
(24) Chen, B.; Zhao, X.; Putkham, A.; Hong, K.; Lobkovsky, E. B.; Hurtado, E. J.; Fletcher, A. J.; Thomas, K. M. *J. Am. Chem. Soc.* **2008**, *130*, 6411.
(25) Forrest, K. A.; Pham, T.; Hogan, A.; McLaughlin, K.; Tudor, B.; Nugent, P.; Burd, S. D.; Mullen, A.; Cioce, C. R.; Wojtas, L.; Zaworotko, M. J.; Space, B. *J. Phys. Chem. C* **2013**, *117*, 17687.
(26) Jin, N.; Seo, J.; Hong, K.; Chun, H. *Microporous Mesoporous Mater.* **2012**, *150*, 32.
(27) Qi, X.-L.; Liu, S.-Y.; Lin, R.-B.; Liao, P.-Q.; Ye, J.-W.; Lai, Z.; Guan, Y.; Cheng, X.-N.; Zhang, J.-P.; Chen, X.-M. *Chem. Commun.* **2013**, *49*, 6864.
(28) Zou, Y.; Hong, S.; Park, M.; Chun, H.; Lah, M. S. *Chem. Commun.* **2007**, 5182.
(29) Dybtsev, D. N.; Chun, H.; Yoon, S. H.; Kim, D.; Kim, K. *J. Am. Chem. Soc.* **2003**, *126*, 32.
(30) Schlueter, J. A.; Geiser, U. *Acta Crystallogr., Sect. C: Cryst. Struct. Commun.* **2004**, *60*, M10.
(31) *Apex2*; Bruker AXS Inc.: Madison, WI, 2007.
(32) Sheldrick, G. M. *SHELXS-2013*; University of Gottingen: Gottingen, Germany, 2013.
(33) Sheldrick, G. M. *SHELXL-2013*; University of Gottingen: Gottingen, Germany, 2013.
(34) Studer, A. J.; Hagen, M. E.; Noakes, T. J. *Phys. B* **2006**, *385*−*86*, 1013.
(35) Larson, A.; von Dreele, R. *General Structure Analysis System (GSAS)*; Los Alamos National Laboratory: Los Alamos, NM, 2000.
(36) Toby, B. *J. Appl. Crystallogr.* **2001**, *34*, 210.
(37) Momma, K.; Izumi, F. *J. Appl. Crystallogr.* **2011**, *44*, 1272.
(38) Dubbeldam, D.; Calero, S.; Ellis, D. E.; Snurr, R. Q. *RASPA 1.0*; Northwestern University: Evanston, IL, 2008.
(39) Haranczyk, M.; Rycroft, C. H.; Martin, R. L.; Willems, T. F. *Zeo ++ 0.1.0*; Lawrence Berkeley National Laboratory: Berkeley, CA, 2012.
(40) Turner, D. R.; Chesman, A. S. R.; Murray, K. S.; Deacon, G. B.; Batten, S. R. *Chem. Commun.* **2011**, *47*, 10189.
(41) Britt, D.; Furukawa, H.; Wang, B.; Glover, T. G.; Yaghi, O. M. *Proc. Natl. Acad. Sci. U.S.A.* **2009**, *106*, 20637.
(42) Chui, S. S. Y.; Lo, S. M. F.; Charmant, J. P. H.; Orpen, A. G.; Williams, I. D. *Science* **1999**, *283*, 1148.
(43) Gelb, L. D.; Gubbins, K. E. *Langmuir* **1999**, *15*, 305.
(44) Rappe, A. K.; Casewit, C. J.; Colwell, K. S.; Goddard, W. A.; Skiff, W. M. *J. Am. Chem. Soc.* **1992**, *114*, 10024.
(45) Uemura, K.; Maeda, A.; Maji, T. K.; Kanoo, P.; Kita, H. *Eur. J. Inorg. Chem.* **2009**, *2009*, 2329.
(46) Nelson, A. P.; Farha, O. K.; Mulfort, K. L.; Hupp, J. T. *J. Am. Chem. Soc.* **2009**, *131*, 458.
(47) Kumar, A. V. A.; Jobic, H.; Bhatia, S. K. *J. Phys. Chem. B* **2006**, *110*, 16666.
(48) Babarao, R.; Jiang, J. W. *Langmuir* **2008**, *24*, 6270.

(49) Yang, S. H.; Sun, J. L.; Ramirez-Cuesta, A. J.; Callear, S. K.; David, W. I. F.; Anderson, D. P.; Newby, R.; Blake, A. J.; Parker, J. E.; Tang, C. C.; Schroder, M. *Nat. Chem.* **2012**, *4*, 887.
(50) Babarao, R.; Hu, Z.; Jiang, J.; Chempath, S.; Sandler, S. I. *Langmuir* **2006**, *23*, 659.
(51) Yang, Q.; Zhong, C. *J. Phys. Chem. B* **2006**, *110*, 17776.
(52) Bae, Y. S.; Mulfort, K. L.; Frost, H.; Ryan, P.; Punnathanam, S.; Broadbelt, L. J.; Hupp, J. T.; Snurr, R. Q. *Langmuir* **2008**, *24*, 8592.
(53) Dietzel, P. D. C.; Johnsen, R. E.; Fjellvåg, H.; Bordiga, S.; Groppo, E.; Chavan, S.; Blom, R. *Chem. Commun.* **2008**, 5125.
(54) Wu, H.; Simmons, J. M.; Srinivas, G.; Zhou, W.; Yildirim, T. *J. Phys. Chem. Lett.* **2010**, *1*, 1946.
(55) Queen, W. L.; Brown, C. M.; Britt, D. K.; Zajdel, P.; Hudson, M. R.; Yaghi, O. M. *J. Phys. Chem. C* **2011**, *115*, 24915.
(56) Ogilvie, S. H.; Duyker, S. G.; Southon, P. D.; Peterson, V. K.; Kepert, C. J. *Chem. Commun.* **2013**, *49*, 9404.